

Simultaneous Inference of Neutron Star Equation of State and Hubble Constant with a Population of Merging Neutron Stars

Tathagata Ghosh ¹, Bhaskar Biswas ^{1,2} and Sukanta Bose^{1,3}

¹*Inter-University Centre for Astronomy and Astrophysics, Post Bag 4, Ganeshkhind, Pune 411 007, India*

²*The Oskar Klein Centre, Department of Astronomy, Stockholm University, AlbaNova, SE-10691 Stockholm, Sweden*

³*Department of Physics & Astronomy, Washington State University, 1245 Webster, Pullman, WA 99164-2814, U.S.A*

(Dated: March 23, 2022)

We develop a method for implementing a proposal on utilizing knowledge of neutron star (NS) equation of state (EoS) for inferring the Hubble constant from a population of binary neutron star (BNS) mergers. This method is useful in exploiting BNSs as standard sirens when their redshifts are unavailable. Gravitational wave (GW) signals from compact object binaries provide a direct measurement of their luminosity distances, but not the redshifts. Unlike in the past, we employ a realistic EoS parameterization in a Bayesian framework to simultaneously measure the Hubble constant and refine the constraints on the EoS parameters. The uncertainty in the redshift depends on the uncertainty in EoS and mass parameters estimated from GW data. Combining the inferred BNS redshifts with the corresponding luminosity distances, one constructs a redshift-distance relationship and deduces the Hubble constant from it. Here, we show that in the Cosmic Explorer era, one can measure the Hubble constant to a precision of $\sim 3\%$ (with a 90% credible interval) with a realistic distribution of thousand BNSs, while allowing for uncertainties in their EoS parameters. The methodology implemented in this work demonstrates a comprehensive algorithm to infer NS EoS and the Hubble constant by simultaneously combining GW observations from merging NSs, choosing a simple population model of NS masses and keeping the merger rate of NSs constant. This method can be immediately extended to incorporate merger rate, population properties, and different cosmological parameters.

I. INTRODUCTION

Gravitational Wave (GW) observations of compact binary coalescences (CBC) have opened a new era of precision cosmology. One of the key goals is to measure the Hubble constant (denoted by H_0), the current expansion rate of the Universe. GW allows the direct measurement of luminosity distance. Additionally, if the redshifts of GW sources are available from any other observations, the Hubble constant can be estimated from the distance-redshift relation. In the absence of an electromagnetic (EM) counterpart, the Hubble constant can be measured using statistical correlation [1–4] of distance with an ensemble of potential host galaxies within the GW event localization uncertainty region. The first ever multi-messenger detection of binary neutron star (BNS) merger GW170817 [5] by the Advanced LIGO [6] and Advanced Virgo detectors [7], with unique identification of host galaxy NGC 4993, is the first standard siren used for the measurement of the Hubble constant $H_0 = 70_{-8}^{+12}$ km s⁻¹ Mpc⁻¹ [8]. However, it is not clear what fraction of BNSs observed in GWs may have EM counterparts that yield a precise redshift measurement, especially at large distances. In this work, we make the conservative assumption that this fraction is small [8, 9].

Apart from bright sirens, like GW170817, H_0 can also be estimated from dark sirens, which lack confirmed EM counterparts. The LIGO-Virgo-KAGRA collaboration recently published the updated measurements of the Hubble constant [10] using 47 GW events from GWTC-3 [11] to be 68_{-8}^{+12} km s⁻¹ Mpc⁻¹ and 68_{-6}^{+8} km s⁻¹ Mpc⁻¹ following two different methods, as

described in Ref. [12] and Ref. [4], respectively. These recent measurements are clearly an improvement compared to the previous estimate of $H_0 = 69_{-8}^{+16}$ km s⁻¹ Mpc⁻¹ – from observations during the O1-O2 runs [13]. Unsurprisingly, all of these GW constraints on H_0 have significant contribution from the observations of GW170817 and its EM counterpart. More instances of independent measurements of luminosity distance and redshift from a wide distribution of sources would be useful toward a resolution of the current discrepancy in H_0 measurements from the early and late-time universe [14].

Messenger and Read [15] proposed an alternative idea of determining the redshift of a binary neutron star (BNS) merger in a GW observation by using prior knowledge of the neutron star (NS) equation of state (EoS). The phase $\Psi(f)$ of the frequency domain GW waveform, $\tilde{h}(f) = A(f)e^{-i\Psi(f)}$ (where $A(f)$ is the amplitude of GW waveform at frequency f), has two components: one is the standard post-Newtonian point-particle frequency domain phase $\Psi_{\text{PP}}(f)$ and the other is the tidal phase component $\Psi_{\text{tidal}}(f)$ due to the tidal deformability of neutron star i.e., $\Psi(f) = \Psi_{\text{PP}}(f) + \Psi_{\text{tidal}}(f)$. Ψ_{PP} depends on redshifted chirp-mass and luminosity distance, in contrast to Ψ_{tidal} is redshift invariant [15]. The degeneracy between mass parameters and the redshift can be broken, if we know the EoS of NSs. This technique is especially useful when the BNS is not accompanied by an electromagnetic counterpart to infer redshift directly. This method neither depends on the observation of EM counterpart nor the identification of potential host galaxies for statistical cross-correlation methods.

Recent progress was reported by Chatterjee *et al.* [16]

by building on the basic concept proposed in Ref. [15]. Their key idea was to use binary Love relations [17] to capture information about NS EoS in a single tidal parameter and use it to constrain the Hubble constant. In this work, we too follow Ref. [15] but use a Hybrid Nuclear plus piecewise-polytrope (PP) parameterization to model the NS EoS [18, 19]. In this EoS model, at low densities of NS, the nuclear empirical parameters are used to construct the EoS model. These nuclear empirical parameters (*e.g.*, nuclear symmetry energy) can be constrained from laboratory experiments and astrophysical observation of neutron stars. The NS EoS, however, is less well understood at densities that are about a couple of times the nuclear saturation density or higher. In these regions, we use the three-piece PP model. We will briefly discuss the EoS model in the next section.

The structure of the paper is as follows. Sec. II introduces the construction of the EoS model. In Sec. III, we describe the Bayesian framework to infer the Hubble constant. In Sec. IV and Sec. V, we discuss the required simulation and the result, respectively. For our simulations, we assume Λ CDM cosmology with $\Omega_m = 0.3$ and $H_0 = 70 \text{ km s}^{-1} \text{ Mpc}^{-1}$ as *true* cosmology throughout the work.

II. EOS MODEL: HYBRID NUCLEAR+PP

In this section, we briefly introduce hybrid nuclear+PP EoS parameterization, which has been used in the past [18, 19] to put joint GW-electromagnetic constraints on the properties of neutron stars. This hybrid EoS parameterization is also used to investigate the nature of “mass-gap” object in GW190814 [20]. Since the crust has a very minimal impact [21, 22] on the macroscopic properties of NSs such mass, radius, tidal deformability etc., standard BPS EoS [23] is used to model the crust under this parameterization. Then this fixed crust is joined with the core EoS in a thermodynamically consistent fashion described in Ref. [24]. The core EoS is divided into two parts:

1. EoS around the nuclear saturation density (ρ_0) is well described via the parabolic expansion of energy per nucleon

$$e(\rho, \delta) \approx e_0(\rho) + e_{\text{sym}}(\rho)\delta^2, \quad (1)$$

where $e_0(\rho)$ is the energy of symmetric nuclear matter for which the number of protons is equal to the number of neutrons, e_{sym} is the energy of the asymmetric nuclear matter (commonly referred as ‘symmetry energy’ in literature), and $\delta \equiv \frac{\rho_p - \rho_n}{\rho_p + \rho_n}$ (where ρ_n, ρ_p being the number density of neutron and proton respectively) is the measure of asymmetry in the number density of neutrons and protons. Around ρ_0 , these two energies can be further

expanded in a Taylor series:

$$e_0(\rho) = e_0(\rho_0) + \frac{K_0}{2}\chi^2 + \dots, \quad (2)$$

$$e_{\text{sym}}(\rho) = e_{\text{sym}}(\rho_0) + L\chi + \frac{K_{\text{sym}}}{2}\chi^2 \dots, \quad (3)$$

where $\chi \equiv (\rho - \rho_0)/3\rho_0 \ll 1$. We truncate the Taylor expansion up to the second order in χ as we use this expansion only up to $1.25\rho_0$. The lowest order parameters are experimentally well constrained and therefore, we fix them at their median values such as $e_0(\rho_0) = -15.9 \text{ MeV}$, and $\rho_0 = 0.16 \text{ fm}^{-3}$. Therefore, the free parameters of this nuclear-physics informed model are the curvature of symmetric matter K_0 , nuclear symmetry energy e_{sym} , slope L , and curvature of symmetric energy K_{sym} . A survey based on 53 experimental results performed in 2016 [25] found of values of $e_{\text{sym}}(\rho_0) = 31.7 \pm 3.2 \text{ MeV}$ and $L = 58.7 \pm 28.1 \text{ MeV}$.

2. At higher densities *i.e.* above $1.25\rho_0$, empirical parameterization starts to break down and we use a three-piece piecewise-polytrope (Γ_1, Γ_2 , and Γ_3 are being the polytropic indices) parameterization divided by the fixed transition densities at $10^{14.7} \text{ gm/cm}^3$ and 10^{15} gm/cm^3 respectively.

Instead of using all the EoS parameters explicitly, we will generally use $\mathcal{E} = \{K_0, e_{\text{sym}}, L, K_{\text{sym}}, \Gamma_1, \Gamma_2, \Gamma_3\}$ later on. In our work, we consider this particular EoS model to constrain the cosmological parameters. In the future, different choice of EoS parameterization or even EoS-insensitive approach [26] can be explored for applying this methodology.

III. METHODOLOGY

GW observations provide mass estimation in detector-frame, *i.e.*, source-frame mass m is observed as redshifted mass, defined as $m^z = m(1+z)$, where z is the redshift of the source. Contrastingly, tidal deformability measurements of a BNS merger from GW observation depend on the source-frame mass pair. As the detector-frame masses are well estimated from lower-PN order terms, tidal deformability can provide the redshift information if we know the EoS [15]. Now, the redshift of the source, as obtained from the detector-frame mass and tidal deformability measurement using the prior information of EoS, combined with the luminosity distance, can infer the Hubble constant. However, it is pretty challenging to know the exact EoS of NS. We can expect that the EoS of NS will be well constrained by the third generation GW detectors, Cosmic Explorer (CE) [27] and Einstein Telescope (ET) [28]. Nevertheless, there will always be some uncertainty in the EoS parameters, even in the third generation detector era [27, 28]. We outline a Bayesian framework to infer the cosmological parameters from GW observation of BNS with the knowledge of EoS, which allows for realistic uncertainties in EoS

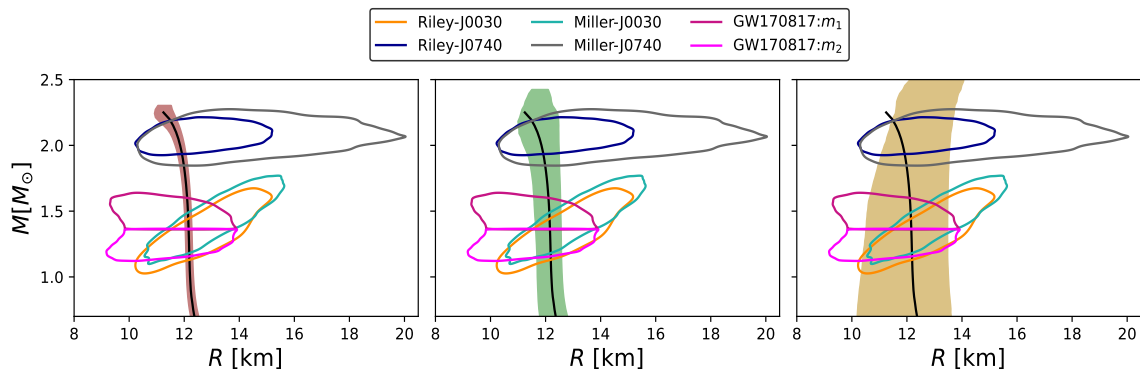


FIG. 1. Mass-radius uncertainty plots corresponding to three different choices of EoS parameter uncertainties, as described in Table I. The solid black line corresponds to the injected EoS.

TABLE I. Different choices of uncertainties in EoS parameters that we use to establish the effectiveness of our method, as described in Sec. II. Here $\mathcal{N}(\mu, \sigma)$ refers to the Gaussian distribution with mean μ and standard deviation σ .

EoS Parameters	Injected	Prior 1	Prior 2	Prior 3
K_0 [MeV]	240	$\mathcal{N}(240, 2.5)$	$\mathcal{N}(240, 20)$	$\mathcal{N}(240, 30)$
e_{sym} [MeV]	31.7	$\mathcal{N}(31.7, 0.5)$	$\mathcal{N}(31.7, 2.5)$	$\mathcal{N}(31.7, 3.2)$
L [MeV]	58.7	$\mathcal{N}(58.7, 1.5)$	$\mathcal{N}(58.7, 5)$	$\mathcal{N}(58.7, 28.1)$
K_{sym} [MeV]	-100	$\mathcal{N}(-100, 2.5)$	$\mathcal{N}(-100, 50)$	$\mathcal{N}(-100, 100)$
Γ_1	2.5	$\mathcal{N}(2.5, 0.05)$	$\mathcal{N}(2.5, 0.2)$	$\mathcal{N}(2.5, 0.5)$
Γ_2	3.5	$\mathcal{N}(3.5, 0.05)$	$\mathcal{N}(3.5, 0.2)$	$\mathcal{N}(3.5, 0.5)$
Γ_3	3.0	$\mathcal{N}(3.0, 0.5)$	$\mathcal{N}(3.0, 2.0)$	$\mathcal{N}(3.0, 2.5)$

parameters. We have assumed some priors for EoS parameters in this work. The prior EoS has been utilized to

infer H_0 and simultaneously refine the constraints on EoS parameters. The joint posterior of the Hubble constant and EoS parameters is given by

$$p(H_0, \mathcal{E} | \{x_{GW}\}) \propto \prod_{i=1}^{N_{det}} \frac{\pi(H_0)}{\beta(H_0)} \pi(\mathcal{E}) \iiint p(x_{GW_i} | m_1^z(m_1, z), m_2^z(m_2, z), \Lambda_1(m_1, \mathcal{E}), \Lambda_2(m_2, \mathcal{E}), d_L(z, H_0)) \times \pi(m_1, m_2 | \mathcal{E}) \pi(z) dz dm_1 dm_2, \quad (4)$$

where $m_{1,2}^z$ is the detector-frame (redshifted) mass of BNS corresponding to source-frame mass $m_{1,2}$ at redshift z ; $\Lambda_{1,2}$ is the tidal deformability, d_L is the luminosity of the source at z for a given value of the Hubble constant H_0 . $\pi(H_0)$, $\pi(\mathcal{E})$ and $\pi(z)$ represent the prior distribution over the Hubble constant, EoS parameters and redshift respectively. $\pi(m_1, m_2 | \mathcal{E})$ is the prior distribution over the source-frame component masses determined from the NS population model. In our work, the population model of BNSs is chosen to be a simple flat distribution over the masses, defined in Eq. 5. $\beta(H_0)$ is the normalization term to ensure that the GW likelihood term $p(x_{GW} | m_1^z, m_2^z, \Lambda_1, \Lambda_2, d_L)$ will be unity when inte-

grated all observable sources. A detail derivation of the Bayesian framework is described in Appendix A.

$$p_{pop}(m | \mathcal{E}) = \begin{cases} \frac{1}{m_{max}(\mathcal{E}) - m_{min}}, & \text{iff } m_{min} \leq m \leq m_{max} \\ 0, & \text{otherwise.} \end{cases} \quad (5)$$

The GW likelihood term $p(x_{GW} | m_1^z, m_2^z, \Lambda_1, \Lambda_2, d_L)$ in Eq. (4) denotes the probability of GW data in presence of signal from BNS merger with parameters redshifted component mass $m_{1,2}^z$, their tidal deformabilities $\Lambda_{1,2}$ and luminosity distance d_L , marginalized over the other parameters of the signal. Using the Bayes theorem, the

posterior for $(m_1^z, m_2^z, \Lambda_1, \Lambda_2, d_L)$ can be written as:

$$p(m_1^z, m_2^z, \Lambda_1, \Lambda_2, d_L | x_{GW}) \propto p(x_{GW} | m_1^z, m_2^z, \Lambda_1, \Lambda_2, d_L) \times \pi(m_1^z, m_2^z, \Lambda_1, \Lambda_2, d_L), \quad (6)$$

where $\pi(m_1^z, m_2^z, \Lambda_1, \Lambda_2, d_L)$ is the prior distribution used to produce the posterior of GW signal parameters. To get the likelihood from the posterior probability, we have to divide out the *prior* $\pi(m_1^z, m_2^z, \Lambda_1, \Lambda_2, d_L)$. We have considered uniform prior over $\Lambda_{1,2}$, chirp-mass in detector frame $\mathcal{M}_c^z = \frac{(m_1 m_2)^{3/5}}{(m_1 + m_2)^{1/5}}(1 + z)$ and mass-ratio $q = m_2/m_1$ while estimating GW signal parameters. The prior for luminosity distance is uniform in comoving volume. The prior $\pi(m_1^z, m_2^z, \Lambda_1, \Lambda_2, d_L)$ is thus simplified as

$$\pi(m_1^z, m_2^z, \Lambda_1, \Lambda_2, d_L) \propto \pi(m_1^z) \pi(m_2^z) \pi(d_L). \quad (7)$$

Since we have considered observed component mass pair $(m_{1,2}^z)$ of BNS in our Bayesian analysis in Eq. (4), we have to compute the relevant prior distribution over the component observed mass-pair ($\pi(m_1^z)$ and $\pi(m_2^z)$ in Eq. (7)) corresponding to the uniform prior over \mathcal{M}_c^z and q used for constraining the GW signal parameters.

In Eq. (4), the prior over the redshift of the source is represented by $\pi(z)$, taken to be of the form

$$\pi(z) \propto \frac{dV_c}{dz} \frac{R(z)}{1+z}. \quad (8)$$

Here $V_c(z)$ is the comoving volume as a function of redshift and $R(z)$ is the merger rate density. The factor $(1+z)^{-1}$ converts from detector-frame to source-frame time. In general, the merger rate density may be a function of redshift. In our work, we consider $R(z)=\text{constant}$, i.e., the BNS distribution is considered to be uniform in comoving volume and source-frame time throughout this work. We consider uniform prior for m_1 and H_0 in Eq. (4) to constraint the Hubble constant and EoS parameters simultaneously. Since m_1 and m_2 are strongly correlated, random choice of m_1 and m_2 as priors makes the Bayesian analysis computationally very expensive. We first create the sample space of observed chirp-mass from its posterior, obtained from GW observation. We then generate samples of m_2^z , and hence m_2 , using the samples of m_1 and z . The chirp-mass is a well measured quantity from GW observation. So, the observed chirp-mass (\mathcal{M}_c^z) will be estimated with high precision during the 3rd generation detector era. We generated m_2 sample in this manner to increase the computational speed.

In Eq. (4), the normalization term $\beta(H_0)$, defined in Eq. (9) encodes the selection effect [2, 29], where p_{det} denotes the detection probability of any GW event. The detail calculation of p_{det} has been discussed in Appendix B.

$$\beta(H_0) = \int p_{det}(z, H_0) \pi(z) dz. \quad (9)$$

While calculating the selection effect, we should ideally consider the effect of the uncertainty in EoS parameters and the population of BNS as p_{det} depends on the

properties of GW source population. The uncertainty in EoS parameters also affects the mass distribution, as maximum mass depends on the values of EoS parameters. The effect of tidal deformability on the amplitude of the gravitational wave signal is small [30, 31]. So, we have fixed the EoS parameters at the injection values and hence we also have the fixed maximum mass ($\approx 2.27M_\odot$) corresponding to injected EoS parameters. For simplicity, we assume that the population properties are known exactly. However, it will be a good exercise to include the uncertainties in the properties of the GW source population for future work. We prepare the mock GW catalog assuming the masses of BNSs follow uniform distribution in the source frame between $m_{\min} \leq m_2 < m_1 \leq m_{\max}$ (discussed in Sec. IV). It is clear from Eq. (5) that the population of BNS depends on the minimum and maximum mass of BNS. The minimum and maximum mass are fixed in the simulation. However, the maximum mass is determined by the EoS of NS. Since we do not account for the uncertainty of EoS parameters for estimating the selection effect, the maximum mass is also fixed. So, the population of BNS does not affect the selection effect.

We assumed flat Λ CDM cosmology with H_0 as a free parameter while performing our Bayesian formulation, Eq. (4). In flat Λ CDM universe, the luminosity distance d_L is related to redshift z as

$$d_L(z) = \frac{c(1+z)}{H_0} \int_0^z \frac{dz'}{\sqrt{\Omega_m(1+z')^3 + (1-\Omega_m)}}. \quad (10)$$

We have used `PyMultinest`¹ [32], python based package based on the nested sampling algorithm Multinest to perform the parameter estimation within the Bayesian framework as mentioned in Eq. (4). During this Bayesian analysis, we use the multivariate Gaussian kernel density estimator from `statsmodels`² [33] to calculate the GW likelihood term.

IV. SIMULATION

We test the method described in Sec. III to several simulated GW events. We have first created a mock GW catalog by injecting the sources uniformly over the sky. The redshift distribution of the sources follows Eq. (8) with $R(z)=\text{constant}$, between 1Gpc and 8Gpc. The masses of the BNS mergers follow uniform distribution in the source frame in the range $1M_\odot \leq m_2 < m_1 \leq 2M_\odot$. However, the uniform prior in source-frame mass is not a realistic mass distribution [34]. We consider a uniform distribution over the source-frame mass for simplicity. However, it will be worth applying this methodology to different population models of BNS to under-

¹ <https://johannesbuchner.github.io/PyMultiNest/>

² <https://www.statsmodels.org/>

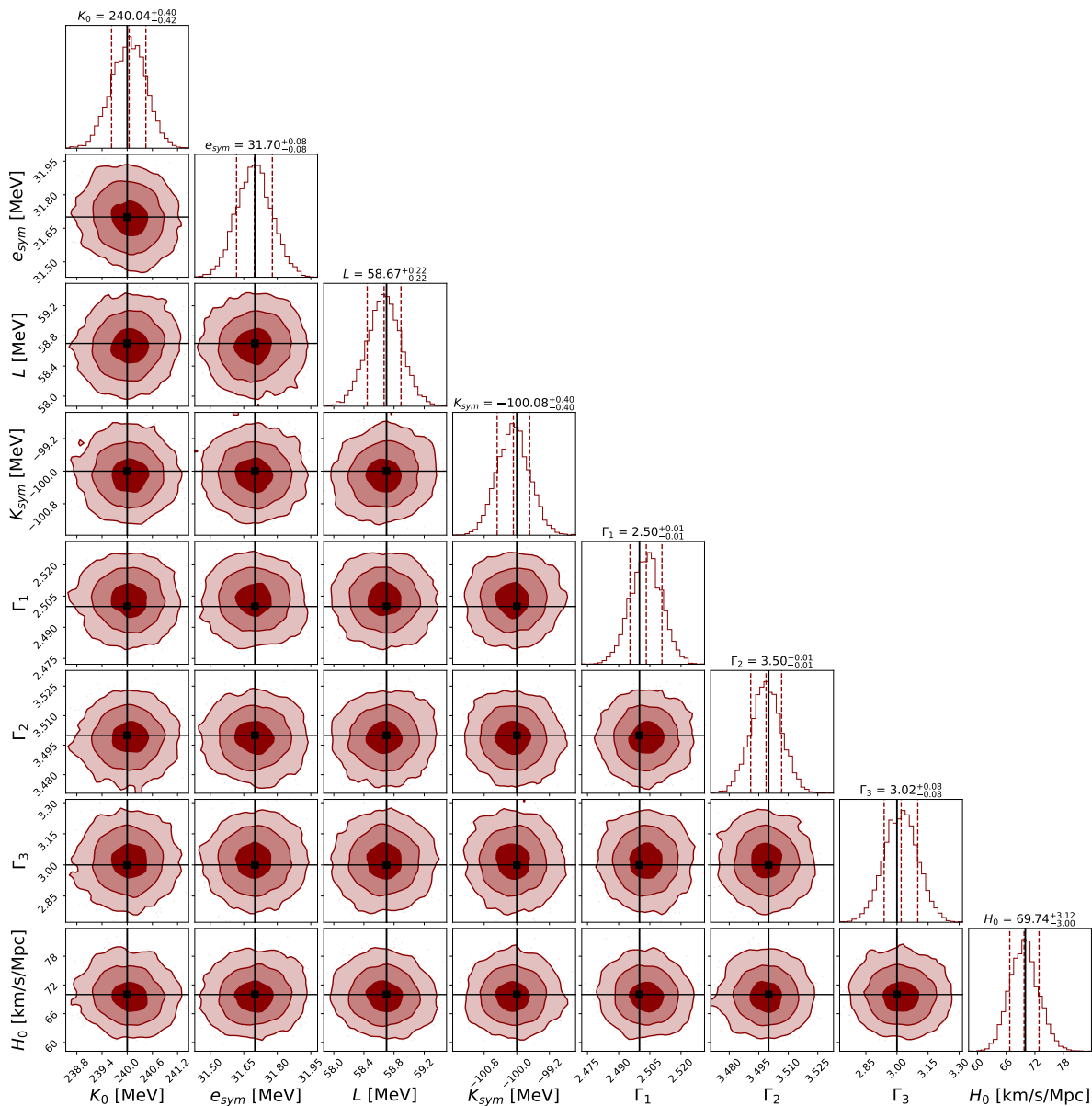


FIG. 2. Constraint of the EoS parameters and H_0 by combining 50 GW events as detected by CE using EoS Prior 1. The black vertical line shows the injected value.

stand the effect of the population in simultaneous inferring the Hubble constant and the EoS parameters. The observed mass from GW observation will be redshifted while observing in the detector-frame. We consider flat Λ CDM cosmology with $\Omega_m = 0.3$ and $H_0 = 70 \text{ km s}^{-1} \text{ Mpc}^{-1}$ to determine the redshift of the GW sources from their luminosity distances. We ignore the spins (set to be 0) of BNS for the present work. Tidal deformability of NS depends on its mass for a particular EoS. The injected values of the EoS parameters are $K_0 = 240 \text{ MeV}$, $e_{sym} = 31.7 \text{ MeV}$, $L = 58.7 \text{ MeV}$ and $K_{sym} = -100 \text{ MeV}$, $\Gamma_1 = 2.5$, $\Gamma_2 = 3.5$ and $\Gamma_3 = 3.0$. In Fig. 1, we show the injected EoS, which is consistent with the constraints of mass-radius measurement from

PSR J0030+0451 [35, 36] and PSR J0740+6620 [37, 38] by NICER collaboration; and GW170817 by LIGO-Virgo observations [39]. We consider CE in our simulation. We inject the synthetic BNS signal of 128 sec to the stationary Gaussian noise realization with Cosmic Explorer (CE) sensitivity³ [40]. Though CE will observe a much longer signal, the tidal effect begins at 5PN is only pronounced close to the merger [15, 16]. We consider the same waveform model IMRPhenomPv2_NRTidal [41] for both the signal injection and recovery of the signal. We

³ <https://dcc.ligo.org/LIGO-T1500293/public>

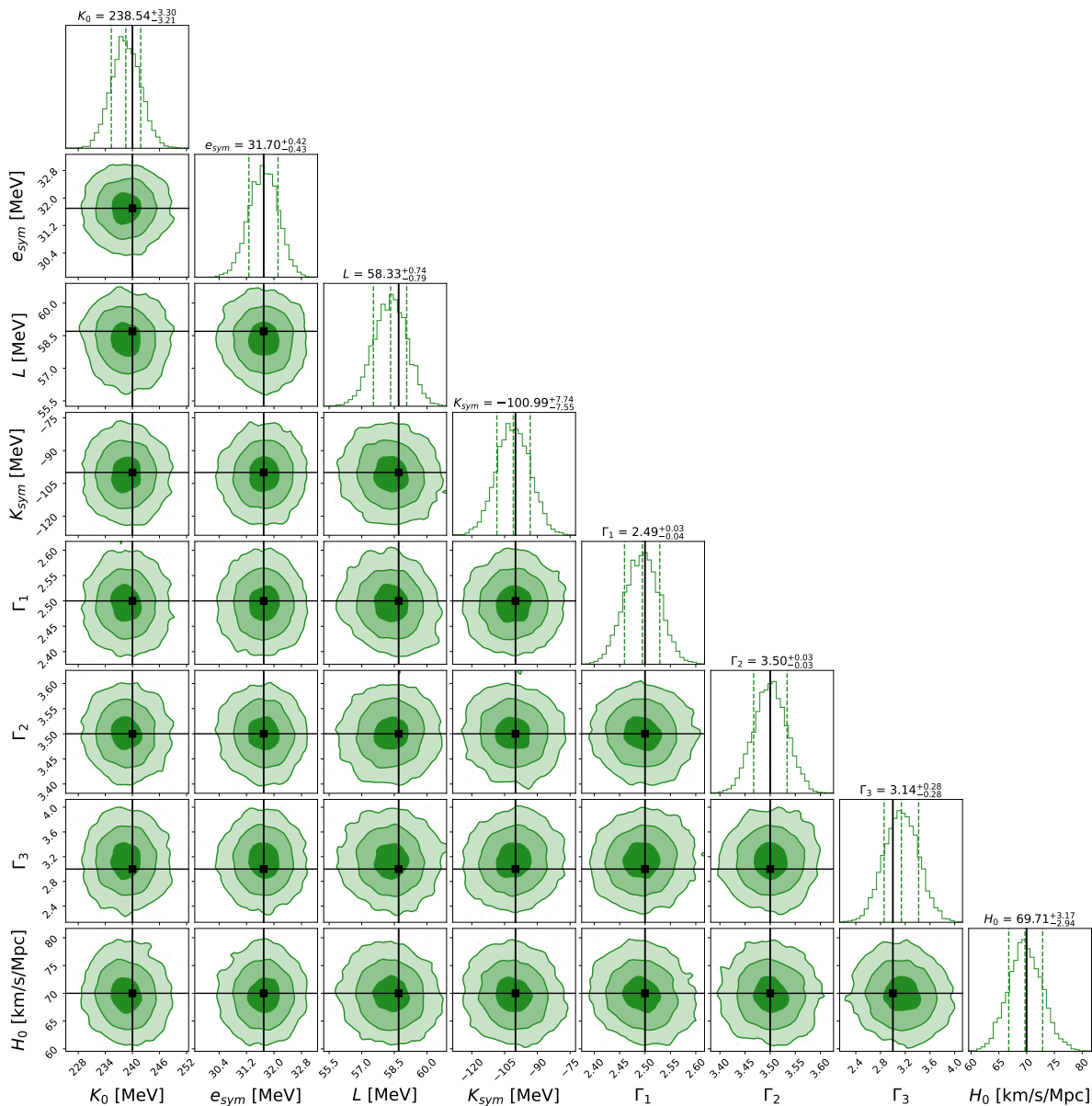


FIG. 3. Constraint of the EoS parameters and H_0 by combining 50 GW events as detected by CE using EoS Prior 2. The black vertical line shows the injected value.

have used `bilby_pipe`⁴, a package for automating the process of running `bilby`⁵ [42] for gravitational wave parameter estimation on computing clusters, to estimate the posterior of the parameters of BNS signal. We performed parameter estimation over mass-pair, tidal deformabilities, luminosity distance and inclination angle. For mass estimation, we consider uniform prior over observed chirp-mass between $(\mathcal{M}_{c,\text{inj}}^z \pm 0.1) M_\odot$ and mass-ratio $q = m_2/m_1$ in $q \in [0.2, 1]$. We use a uniform prior in

tidal deformabilities $\Lambda_{1,2} \in [0, 5000]$. We choose uniform prior in the comoving distance for estimating luminosity distance between 100 Mpc and twice of $d_{L,\text{inj}}$ for luminosity distance estimation and isotropic prior for inclination angle. We fixed the other parameters (sky-position, dimensionless spin magnitudes, tilt angle between their spins, orbital angular momentum, spin vectors describing the azimuthal angle separating the spin vectors, precession angle, polarization angle, coalescence time and its orbital phase at coalescence) at the injected values.

Now, the parameters of the synthetic GW catalog have been used to determine H_0 and the EoS parameters, as discussed in Sec. III. We consider sufficiently large uniform prior over redshift to cover the entire lu-

⁴ <https://pypi.org/project/bilby-pipe/>

⁵ <https://lscsoft.docs.ligo.org/bilby/>

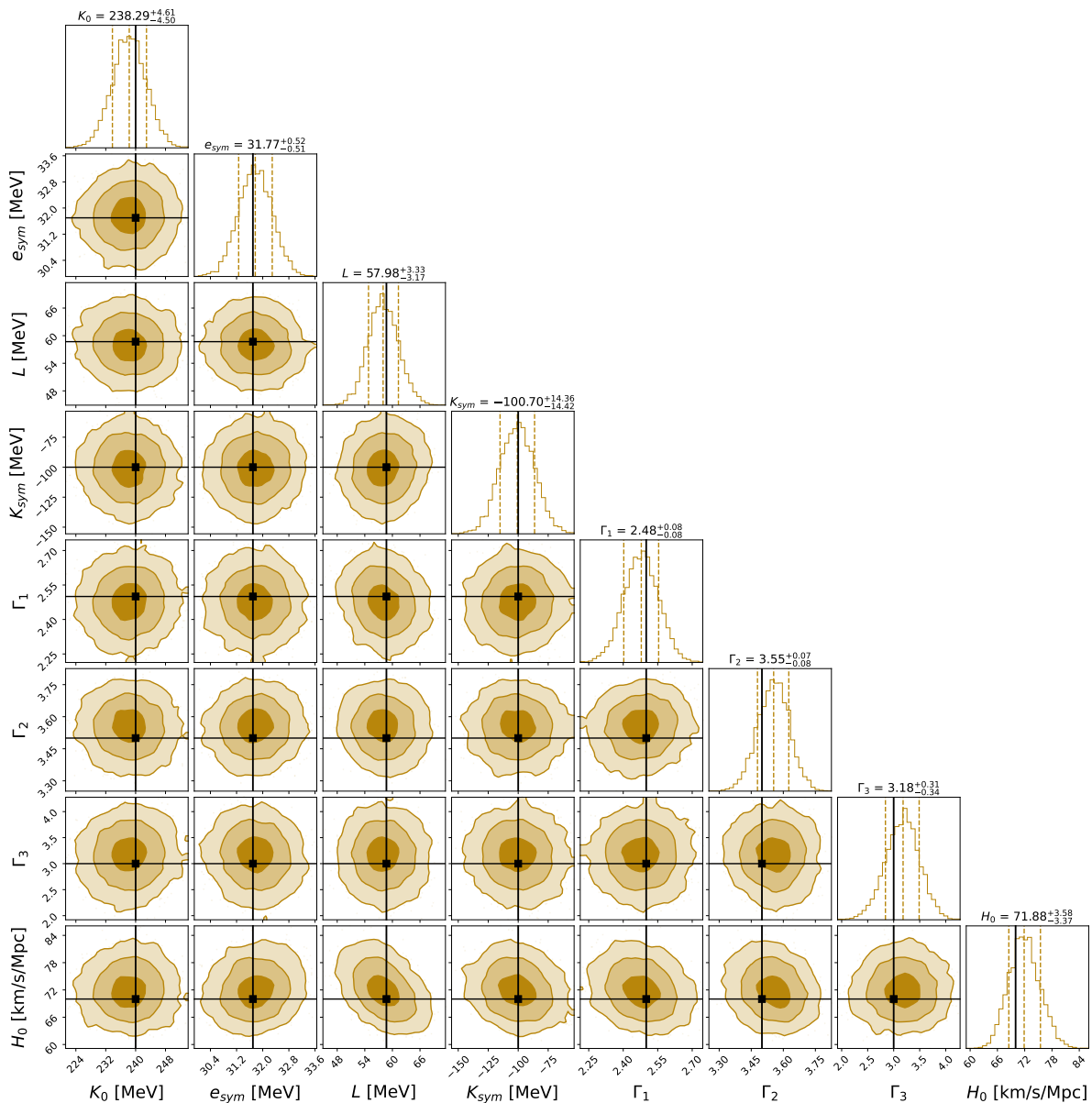


FIG. 4. Constraint of the EoS parameters and the Hubble constant by combining 50 GW events as detected by CE using EoS Prior 3. The black vertical line shows the injected value.

minosity distance posterior obtained from GW observation for any value of H_0 within our prior range between $20 \text{ km s}^{-1} \text{ Mpc}^{-1}$ and $120 \text{ km s}^{-1} \text{ Mpc}^{-1}$. We have already mentioned that we need to assume some uncertainty in the EoS parameters. The projected uncertainty in $R_{1.4}$ measurement is $\sim 1 \text{ km}$ after the fifth observing (O5) run of LIGO-Virgo-KAGRA Network [43]. The expected constraint of NS radius is better than 0.1 km from the GW of BNS as observed by CE [27]. So, we consider three sets of uncertainties in the EoS parameters, mentioned in Table I along with the injected values of the EoS parameters. The uncertainty in $R_{1.4M_\odot}$ corresponding to each of the prior EoS is also mentioned in Table I to reflect the idea of how much uncertainty in the EoS

parameters we are using in this work. The mass-radius plot for all the prior EoSs, shown in Fig. 1 also gives a similar qualitative measurement about the uncertainties in the EoS parameters we are considering in our work. Now, the posterior of Hubble constant along with the EoS parameters have been measured using the redshift information and luminosity distance of GW sources using the Bayesian framework as described above.

V. RESULTS

We apply the method, as described in Sec.III to 50 GW events to test the efficacy of the method to estimate the

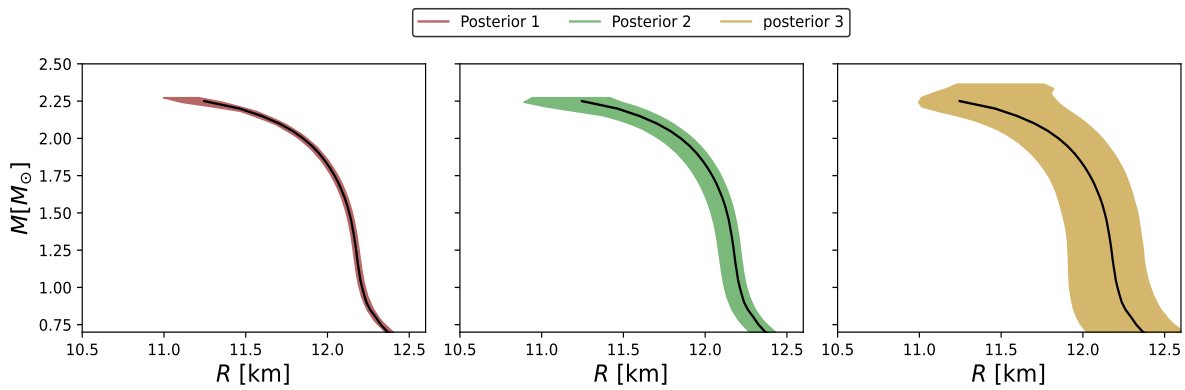


FIG. 5. Mass-radius uncertainty plot for three different choices of the EoS parameters uncertainty as mentioned in Table I. The solid black curve in each plot is the mass-radius plot corresponding to the injected EoS parameters.

TABLE II. Median and 90% credible interval of the EoS Parameters, $R_{1.4}$, R_2 , $\Lambda_{1.4}$, Λ_2 , M_{\max} , skin thickness and the Hubble constant as obtained using our methodology to 50 GW events with EoS Prior 1, Prior 2 and Prior 3, mentioned in Table I. The parameters, such as $R_{1.4}$, R_2 , M_{\max} and skin thickness have been inferred from the injected EoS parameters (K_0 , e_{sym} , L , K_{sym} , Γ_1 , Γ_2 , Γ_3). The injected (or inferred) values of the parameters are also mentioned in the second column.

Parameters	Injected	Posterior 1	Posterior 2	Posterior 3
K_0 [MeV]	240	$240.04^{+0.66}_{-0.70}$	$238.54^{+5.35}_{-5.20}$	$238.29^{+7.47}_{-7.55}$
e_{sym} [MeV]	31.70	$31.70^{+0.13}_{-0.13}$	$31.70^{+0.68}_{-0.71}$	$31.77^{+0.85}_{-0.85}$
L [MeV]	58.70	$58.67^{+0.38}_{-0.38}$	$58.33^{+1.22}_{-1.27}$	$57.98^{+5.63}_{-5.23}$
K_{sym} [MeV]	-100	$-100.08^{+0.67}_{-0.65}$	$-100.99^{+12.68}_{-12.63}$	$-100.70^{+23.53}_{-23.39}$
Γ_1	2.5	$2.50^{+0.01}_{-0.01}$	$2.49^{+0.06}_{-0.06}$	$2.48^{+0.12}_{-0.13}$
Γ_2	3.5	$3.50^{+0.01}_{-0.01}$	$3.50^{+0.06}_{-0.05}$	$3.55^{+0.12}_{-0.13}$
Γ_3	3.0	$3.02^{+0.13}_{-0.14}$	$3.14^{+0.46}_{-0.45}$	$3.18^{+0.52}_{-0.57}$
$R_{1.4M_\odot}$ [km]	12.153	$12.154^{+0.018}_{-0.019}$	$12.130^{+0.067}_{-0.071}$	$12.119^{+0.232}_{-0.224}$
R_{2M_\odot} [km]	11.851	$11.851^{+0.026}_{-0.026}$	$11.852^{+0.010}_{-0.108}$	$11.854^{+0.267}_{-0.283}$
$\Lambda_{1.4M_\odot}$	375.813	$380.478^{+6.326}_{-6.151}$	$375.578^{+15.591}_{-15.431}$	$375.578^{+43.880}_{-39.418}$
Λ_{2M_\odot}	29.33	$29.339^{+0.565}_{-0.560}$	$28.848^{+2.209}_{-2.238}$	$29.718^{+5.608}_{-5.428}$
M_{\max} [M_\odot]	2.271	$2.267^{+0.008}_{-0.014}$	$2.241^{+0.039}_{-0.081}$	$2.240^{+0.080}_{-0.112}$
R_{skin} [fm]	0.1873	$0.1872^{+0.0005}_{-0.0005}$	$0.1867^{+0.0018}_{-0.0019}$	$0.1862^{+0.0083}_{-0.0077}$
H_0 [km s $^{-1}$ Mpc $^{-1}$]	70	$69.74^{+5.16}_{-4.83}$	$69.71^{+5.17}_{-5.05}$	$71.88^{+5.88}_{-5.36}$

EoS parameters and the Hubble constant simultaneously. We consider GW events as detected if the network SNR is equal to or greater than 8. The individual posteriors of the EoS parameters and the Hubble constant may not always be peaked at the true values; some posteriors may be multi-modal also. It is due to the measurement uncertainty of the GW signal parameters. In particular, there exists a degeneracy in the measurability of the luminosity distance and the inclination angle of binaries in GWs [44, 45]; e.g., a source will appear fainter not just when it is farther but also when its orbital plane is more tilted relative to the line of sight (see Ref. [2]). Since the orbit orientations in a population are random,

the expectation is that with an increasing number of observations, this method of combining individual source parameter posteriors will still succeed in constraining H_0 and the EoS parameters with increasing precision since every BNS signal is characterized by the same H_0 and the EoS parameters.

The posteriors of the inferred EoS parameters and H_0 , together with their correlation, are shown in Figs. 2, 3 and 4 corresponding to Priors 1, 2 and 3, respectively. The different choices of priors in the EoS parameters (also discussed in Sec. IV) are mentioned in Table I. We summarize the 90% credible interval of the inferred EoS parameters and Hubble constant in Table II. We

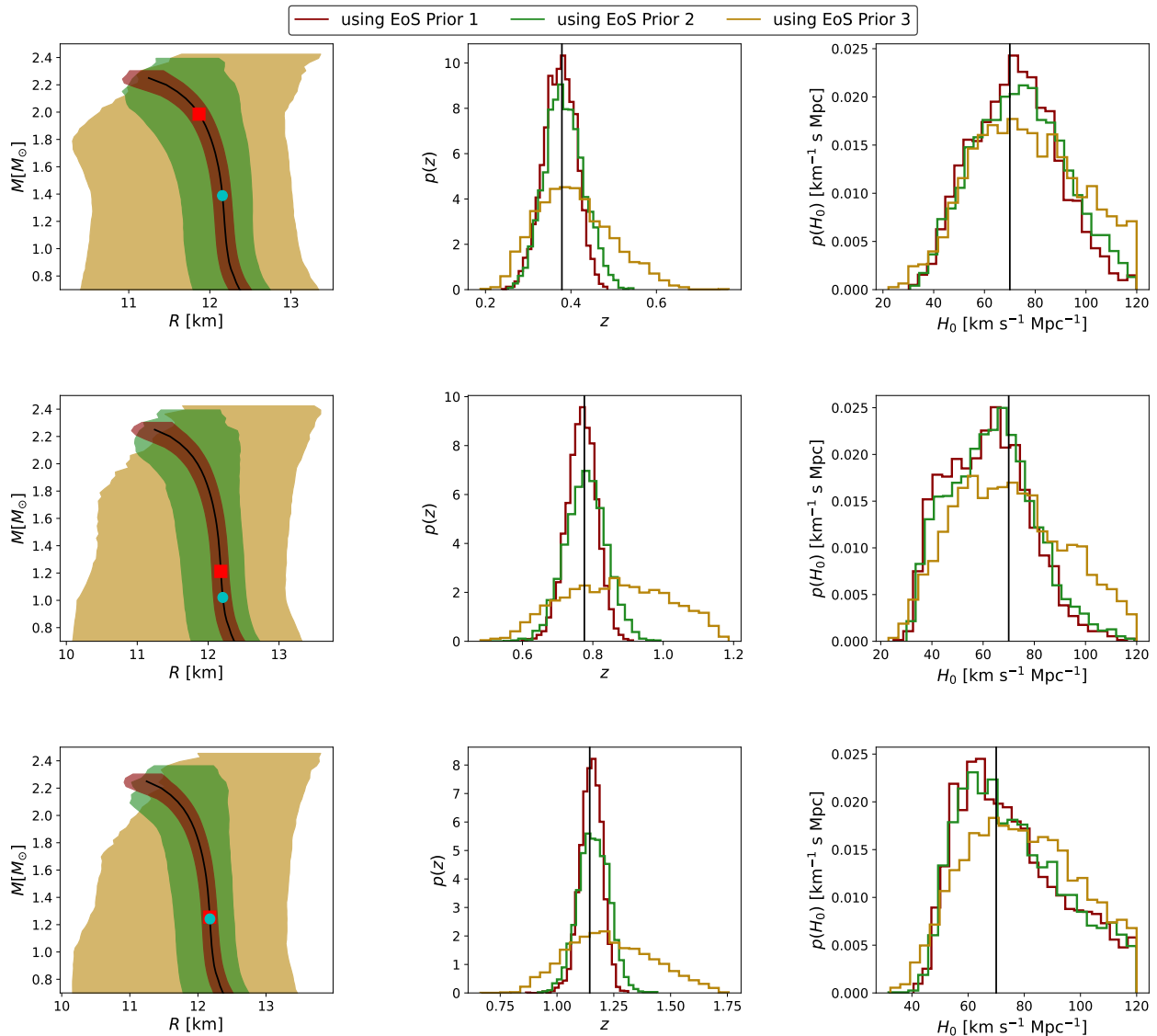


FIG. 6. Uncertainties in the EoS Parameters, redshift and H_0 for three choices of EoS Priors for three different GW events at different distances. Each row corresponds to a single GW event, with the injected redshift is shown by a vertical black line in the middle panel. The vertical black line of all the plots show the injected values corresponding to the parameter at the horizontal axis of that plot. The red-colored square and the cyan-colored round markers refer to the injected BNS event in each of the mass-radius diagrams (first column).

also mention some other inferred parameters from the NS EoS posteriors like $R_{1.4M_\odot}$ (radius of neutron star at $1.4M_\odot$), R_{2M_\odot} , $\Lambda_{1.4M_\odot}$ (tidal deformability of neutron star at $1.4M_\odot$) and Λ_{2M_\odot} in Table II.

From the joint posterior of H_0 and the EoS parameters (see Fig. 2, 3 and 4 and Table II), it is clearly evident that the uncertainty in measurement of the Hubble constant is not significantly different. However, the uncertainties in the posterior of the EoS parameters are quite different: more constrained prior of the EoS parameters yield tighter constraint over the EoS parameters. The mass-

radius plots (see Fig. 5 and Table II for the median values with the 90% credible intervals of EoS parameters) corresponding to three EoS posteriors also reveal that the constraints of the EoS parameters are significantly different. The error in inferring the Hubble constant is limited by the intrinsic degeneracy between luminosity distance and inclination of the GW event. Fig. 6 shows the mass-radius plot, redshift estimation and inferred H_0 for three GW events at different distances. In Fig. 6, the upper panel, middle panel and lower panel correspond to 3 GW events with mass-pairs $(1.98 + 1.39)M_\odot$, $(1.21 + 1.02)M_\odot$

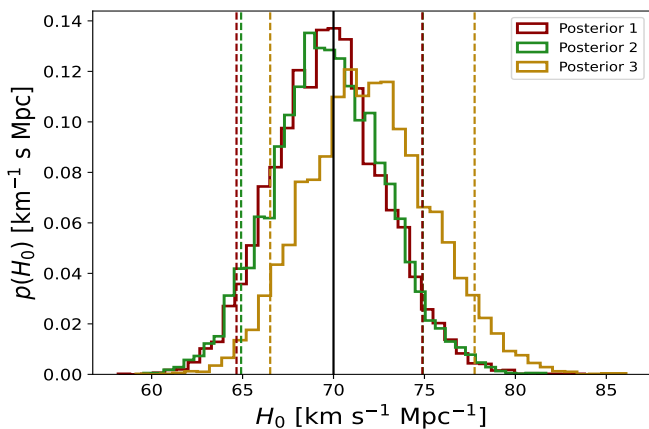


FIG. 7. Comparison of joint estimate of the Hubble constant over 50 GW events for the different choices of EoS. The black vertical line denotes the injected value of $H_0 = 70 \text{ km s}^{-1} \text{ Mpc}^{-1}$. The dashed vertical lines of the same color indicates 90% highest density credible interval corresponding to the histogram of that color.

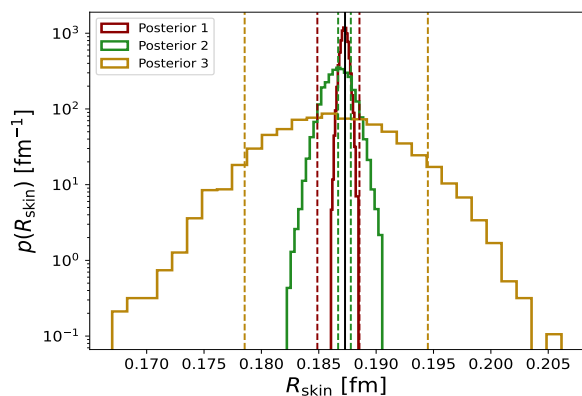


FIG. 8. Estimation of skin thickness for the different choices of the EoS priors. The black vertical line denotes the inferred value of the skin thickness $R_{\text{skin}} = 0.1873 \text{ fm}$ corresponding to injected EoS. The dashed vertical lines of the same color indicates 90% highest density credible interval corresponding to the histogram of that color.

and $(1.25 + 1.24)M_{\odot}$, injected at redshift 0.379, 0.776 and 1.144 respectively. It is noticeable from the mass-radius plots that EoS parameters are constrained significantly while considering tighter priors over EoS parameters. The redshift uncertainties also show the same feature. However, the Hubble constant measurement error is almost similar for EoS Prior 1 and Prior 2. The H_0 posterior is slightly broader for EoS Prior 3 in comparison to Prior 1 and Prior 2. With the given injected population, the estimation of the Hubble constant is not sensitive to the EoS parameters uncertainty. However, we can expect the improvement of the distance-inclination degeneracy measurement from GW signal with the development of

higher mode waveform model of BNS merger [46], leading to a more precise estimation of the Hubble constant.

Chatterjee *et al.* [16] mentioned that $\Delta H_0/H_0 \sim 2\%$ for $N_{\text{det}} = 10^3$ detected GW events observed by CE. They assumed $\sim 1/\sqrt{N_{\text{det}}}$ scaling for estimating the projected uncertainty measurement in the Hubble constant during CE era. We find the 90% confidence-interval error $\Delta H_0/H_0 \sim 14 - 16\%$ (see Fig. 7), depending on the prior EoS, while inferring the Hubble constant from 50 BNS observations. We also estimate the uncertainty with the similar scaling $\sim 1/\sqrt{N_{\text{det}}}$ in the measurement of the Hubble constant $\Delta H_0/H_0 \sim 3\%$ with $N_{\text{det}} = 10^3$ events, depending on the uncertainties in the EoS parameters, based on the constraint of H_0 by combining individual H_0 posterior of 50 GW events. The projected uncertainty in H_0 measurement is slightly greater than the uncertainty estimation of H_0 , mentioned by Chatterjee *et al.* [16]. It is expected because we consider uncertainties in the EoS parameters, unlike Chatterjee *et al.* [16]. However, improvement in the uncertainty due to luminosity distance-inclination angle degeneracy should have a more significant effect in constraining H_0 as discussed above.

Recently, PREX-II collaboration have reported [47] the value of neutron skin thickness of ^{208}Pb to be, $R_{\text{skin}}^{208} = 0.29 \pm 0.07 \text{ fm}$ (mean and 1σ standard deviation). Ref. [48] have argued, this result implies the value of L to be $106 \pm 37 \text{ MeV}$. They also deduce a larger value of NS radius as there exist a correlation between $R_{1.4}$ and L based on relativistic mean field calculation. However, Ref. [19] argued that the measurement uncertainty in R_{skin}^{208} by PREX-II is much broader and astrophysical observations dominate over it after combining. Combined astrophysical observations and PREX-II data yields the value of empirical parameter $L = 69^{+21}_{-19} \text{ MeV}$, $R_{\text{skin}}^{208} = 0.20^{+0.05}_{-0.05} \text{ fm}$, and radius of a $1.4M_{\odot}$ ($R_{1.4}$) = $12.70^{+0.42}_{-0.54} \text{ km}$ at 1σ CI. Nevertheless, a better measurement of R_{skin}^{208} might have a small effect on the radius of low mass NSs, but for the high masses there will be almost no effect. The state-of-the-art chiral effective field theory calculations predict [49] the value of R_{skin} to be $0.17 - 0.18 \text{ fm}$ based on Bayesian analyses using mocked data. Therefore, if the high R_{skin}^{208} values continue to persist with lesser uncertainty, it would pose a challenge to the current theoretical understanding about the nuclear matter near the saturation densities. Following Ref. [19] we estimate the skin thickness R_{skin} using the universal relation from Viñas *et al.* [50] connecting R_{skin} and the empirical parameter L : $R_{\text{skin}}^{208} [\text{fm}] = 0.101 + 0.00147 \times L [\text{MeV}]$. The estimation of skin thickness for the different EoS priors are shown in Fig. 8 and Table II. We find irrespective of the choice in the EoS priors, future observations from CE will constrain R_{skin} with sub-percentage accuracy. So if indeed there is a tension between nuclear theory and astrophysical observations, it will be revealed.

VI. DISCUSSION

In this paper, we demonstrate how a population of BNS can constrain the EoS parameters and the Hubble constant simultaneously during 3rd generation detector era when unique transient electromagnetic counterparts cannot be identified. For dark GW signal from CBC, the current state of the art is to perform a statistical approach by considering the redshifts of all potential host galaxies within the three-dimensional localization region of GW event to get a constraint on the distance-redshift relationship [1–4]. However, our method can infer the redshift information of the GW event from the knowledge of the prior EoS parameters. We combine the redshift information with the luminosity distance measured from GW observation to estimate the Hubble constant.

We have tested our formalism using three different priors of the EoS parameters. We only infer the Hubble constant as the cosmological parameter in our Bayesian analysis. However, the methodology can also be extended to estimate other cosmological parameters, such as matter density and the dark energy equation of state. We can expect a significant constraint on the Hubble constant by 2nd generation detector era (see Ref. [2]). So, one can use constrained prior over the Hubble constant in 3rd detector era. The use of informed H_0 prior may help to estimate other cosmological parameters. We also emphasize the requirement to measure luminosity distance to higher precision, as the Hubble constant measurement uncertainty is strongly affected by the degeneracy between luminosity distance and inclination angle.

We can expect many detections of BNS mergers with 3rd generation detectors in the high redshift. We consider constant merger rate and a simple mass population model of BNS distribution in our work. However, we should consider a realistic merger rate (evolving with redshift) and population model of BNS distribution [51, 52].

$$p(x_{GW}|H_0, \mathcal{E}) \propto \frac{1}{\beta(H_0)} \iiint p(x_{GW_i}|m_1^z(m_1, z), m_2^z(m_2, z), \Lambda_1(m_1, \mathcal{E}), \Lambda_2(m_2, \mathcal{E}), d_L(z, H_0)) \times \pi(m_1, m_2)\pi(z)dzdm_1dm_2 \quad (\text{A2})$$

In terms of explicit parameters, Eq. (A) can conveniently be written as

$$p(x_{GW}|H_0, \mathcal{E}) = \frac{1}{\beta(H_0)} \iiint p(x_{GW_i}|z, m_1, m_2, \mathcal{E}, H_0) \times \pi(m_1, m_2)\pi(z)dzdm_1dm_2 \quad (\text{A3})$$

where a normalization term $\beta(H_0)$ has been included in the denominator to account for selection effects [2, 29].

Our methodology can easily be extended to incorporate simultaneous inference of other cosmological parameters and more realistic population models of NSs. We leave this work as a future exercise.

In the case of the EoS parameters, other observations can also put stringent measurements of the mass and radii of NSs. In particular, the observation of PSR J0030+0451 [35, 36] PSR J0740+6620 [37, 38] by NICER collaboration has been utilized to measure mass-radius relation of the NS.

ACKNOWLEDGEMENTS

We thank Rana Nandi and Prasanta Char for earlier collaboration (with BB and SB) on the construction of the neutron star equation of state parameterization used here and for useful discussions. We would also like to thank Hsin-Yu Chen for carefully reading the manuscript and making several useful suggestions. TG gratefully acknowledges using the LDG clusters, Sarathi at IUCAA and Hawk at Cardiff University, accessed through the LIGO-Virgo-Kagra Collaboration. We are also grateful for the computational resource Pegasus provided by IUCAA for this work.

Appendix A: Bayesian Framework

From Bayes Theorem, the joint posterior of cosmological parameters and the EoS parameters for a detected GW event $p(H_0, \mathcal{E}|x_{GW})$ is given by

$$p(H_0, \mathcal{E}|x_{GW}) = p(x_{GW}|H_0, \mathcal{E})\pi(H_0)\pi(\mathcal{E}) \quad (\text{A1})$$

The likelihood for a single GW event in Eq. (A1) can be written as

$$\beta(H_0) = \int p_{det}(z, H_0)\pi(z)dz \quad (\text{A4})$$

The term $p_{det}(z, H_0)$ in Eq. (A4) denotes detection probability for a particular choice of redshift and H_0 . We elaborate the calculation of $p_{det}(z, H_0)$ (similar to $p(d_{GW}|z, H_0)$ in Ref. [4]) following Gray *et al.* [4] (implemented in `gwcosmo`⁶).

⁶ gwcosmo code: <https://git.ligo.org/lscsoft/gwcosmo>

The final joint posterior of the Hubble constant and the EoS parameters can be obtained by combining all sources, as follows:

$$p(H_0, \mathcal{E}|\{x_{GW}\}) = \prod_{i=1}^{N_{det}} p(H_0, \mathcal{E}|x_{GW_i}) \quad (\text{A5})$$

Appendix B: Estimation of Detection Probability

The selection effect as defined in Eq. (9) (also in Eq. (A4)) completely depends on GW detection efficiency. GW detector can identify those signals that generate sufficiently high amplitude response. We consider a GW event as detected if the network SNR is some threshold SNR ρ_{th} or higher. In our work, we set $\rho_{th} = 8$. We calculate p_{det} using the injection of BNS signal. We populate 10^3 BNSs uniformly over the entire sky for each of the redshift bin and a given choice of Hubble constant. These BNSs follow the same population model

as we assumed for this work. We have injected the total number of BNS mergers $\sim 10^7$ for the entire range of the Hubble constant and redshift for computing detection probability; among all the sources, $\sim 8 \times 10^6$ sources qualify the detection criterion. We then calculate optimal SNR [53] of the injected GW signal of 128s at each of the detector and hence the network SNR. For this purpose, we have used `bilby` [42] to inject GW signal and calculate optimal SNR. Since, ρ^2 follows non-central chi-squared distribution with two degrees of freedom [54], in the presence of stationary and Gaussian noise with a known power spectrum, we thus estimate the detection probability p_{det} for a certain redshift bin and a particular choice of H_0 by probability density function of non-central chi-squared distribution with degrees of freedom is twice of the number of detectors and non-centrality parameter is ρ_{th} . The detection probability is estimated in the similar way as implemented in `gwcosmo`. Now, it is straight forward to calculate the selection function $\beta(H_0)$ (Eq. 9) by marginalizing the detection probability over the redshift prior used in the Bayesian framework.

-
- [1] B. F. Schutz, *Nature* **323**, 310 (1986).
- [2] H.-Y. Chen, M. Fishbach, and D. E. Holz, *Nature* **562**, 545 (2018), arXiv:1712.06531 [astro-ph.CO].
- [3] M. Fishbach *et al.* (LIGO Scientific, Virgo), *Astrophys. J. Lett.* **871**, L13 (2019), arXiv:1807.05667 [astro-ph.CO].
- [4] R. Gray *et al.*, *Phys. Rev. D* **101**, 122001 (2020), arXiv:1908.06050 [gr-qc].
- [5] B. P. Abbott *et al.* (LIGO Scientific, Virgo), *Phys. Rev. Lett.* **119**, 161101 (2017), arXiv:1710.05832 [gr-qc].
- [6] J. Aasi *et al.* (LIGO Scientific), *Class. Quant. Grav.* **32**, 074001 (2015), arXiv:1411.4547 [gr-qc].
- [7] F. Acernese *et al.* (VIRGO), *Class. Quant. Grav.* **32**, 024001 (2015), arXiv:1408.3978 [gr-qc].
- [8] B. P. Abbott *et al.* (LIGO Scientific, Virgo, 1M2H, Dark Energy Camera GW-E, DES, DLT40, Las Cumbres Observatory, VINROUGE, MASTER), *Nature* **551**, 85 (2017), arXiv:1710.05835 [astro-ph.CO].
- [9] M. Soares-Santos *et al.* (DES, Dark Energy Camera GW-EM), *Astrophys. J. Lett.* **848**, L16 (2017), arXiv:1710.05459 [astro-ph.HE].
- [10] R. Abbott *et al.* (LIGO Scientific, VIRGO, KAGRA), (2021), arXiv:2111.03604 [astro-ph.CO].
- [11] R. Abbott *et al.* (LIGO Scientific, VIRGO, KAGRA), (2021), arXiv:2111.03606 [gr-qc].
- [12] S. Mastrogiovanni, K. Leyde, C. Karathanasis, E. Chassande-Mottin, D. A. Steer, J. Gair, A. Ghosh, R. Gray, S. Mukherjee, and S. Rinaldi, *Phys. Rev. D* **104**, 062009 (2021), arXiv:2103.14663 [gr-qc].
- [13] B. P. Abbott *et al.* (LIGO Scientific, Virgo), *Astrophys. J.* **909**, 218 (2021), arXiv:1908.06060 [astro-ph.CO].
- [14] L. Verde, T. Treu, and A. G. Riess, *Nature Astron.* **3**, 891 (2019), arXiv:1907.10625 [astro-ph.CO].
- [15] C. Messenger and J. Read, *Phys. Rev. Lett.* **108**, 091101 (2012), arXiv:1107.5725 [gr-qc].
- [16] D. Chatterjee, A. H. K. R., G. Holder, D. E. Holz, S. Perkins, K. Yagi, and N. Yunes, *Phys. Rev. D* **104**, 083528 (2021), arXiv:2106.06589 [gr-qc].
- [17] K. Yagi and N. Yunes, *Class. Quant. Grav.* **33**, 13LT01 (2016), arXiv:1512.02639 [gr-qc].
- [18] B. Biswas, P. Char, R. Nandi, and S. Bose, *Phys. Rev. D* **103**, 103015 (2021), arXiv:2008.01582 [astro-ph.HE].
- [19] B. Biswas, *Astrophys. J.* **921**, 63 (2021), arXiv:2105.02886 [astro-ph.HE].
- [20] B. Biswas, R. Nandi, P. Char, S. Bose, and N. Stergioulas, *Mon. Not. Roy. Astron. Soc.* **505**, 1600 (2021), arXiv:2010.02090 [astro-ph.HE].
- [21] R. Gamba, J. S. Read, and L. E. Wade, *Class. Quant. Grav.* **37**, 025008 (2020), arXiv:1902.04616 [gr-qc].
- [22] B. Biswas, R. Nandi, P. Char, and S. Bose, *Phys. Rev. D* **100**, 044056 (2019), arXiv:1905.00678 [gr-qc].
- [23] G. Baym, C. Pethick, and P. Sutherland, *Astrophys. J.* **170**, 299 (1971).
- [24] W.-J. Xie and B.-A. Li, *Astrophys. J.* **883**, 174 (2019), arXiv:1907.10741 [astro-ph.HE].
- [25] M. Oertel, M. Hempel, T. Klöhn, and S. Typel, *Rev. Mod. Phys.* **89**, 015007 (2017), arXiv:1610.03361 [astro-ph.HE].
- [26] B. Biswas and S. Datta, (2021), arXiv:2112.10824 [astro-ph.HE].
- [27] M. Evans *et al.*, (2021), arXiv:2109.09882 [astro-ph.IM].
- [28] M. Maggiore *et al.*, *JCAP* **03**, 050 (2020), arXiv:1912.02622 [astro-ph.CO].
- [29] I. Mandel, W. M. Farr, and J. R. Gair, *Mon. Not. Roy. Astron. Soc.* **486**, 1086 (2019), arXiv:1809.02063 [physics.data-an].
- [30] B. P. Abbott *et al.* (LIGO Scientific, Virgo), *Class. Quant. Grav.* **37**, 045006 (2020), arXiv:1908.01012 [gr-qc].
- [31] K. Chatziioannou, *Gen. Rel. Grav.* **52**, 109 (2020), arXiv:2006.03168 [gr-qc].
- [32] J. Buchner, A. Georgakakis, K. Nandra, L. Hsu, C. Rangel, M. Brightman, A. Merloni, M. Salvato,

- J. Donley, and D. Kocevski, *Astron. Astrophys.* **564**, A125 (2014), arXiv:1402.0004 [astro-ph.HE].
- [33] S. Seabold and J. Perktold, in *9th Python in Science Conference* (2010).
- [34] R. Abbott *et al.* (LIGO Scientific, VIRGO, KAGRA), (2021), arXiv:2111.03634 [astro-ph.HE].
- [35] T. E. Riley *et al.*, *Astrophys. J. Lett.* **887**, L21 (2019), arXiv:1912.05702 [astro-ph.HE].
- [36] M. C. Miller *et al.*, *Astrophys. J. Lett.* **887**, L24 (2019), arXiv:1912.05705 [astro-ph.HE].
- [37] T. E. Riley *et al.*, *Astrophys. J. Lett.* **918**, L27 (2021), arXiv:2105.06980 [astro-ph.HE].
- [38] M. C. Miller *et al.*, *Astrophys. J. Lett.* **918**, L28 (2021), arXiv:2105.06979 [astro-ph.HE].
- [39] B. P. Abbott *et al.* (LIGO Scientific, Virgo), *Phys. Rev. Lett.* **121**, 161101 (2018), arXiv:1805.11581 [gr-qc].
- [40] B. P. Abbott, R. Abbott, T. D. Abbott, M. R. Abernathy, K. Ackley, C. Adams, P. Addesso, R. X. Adhikari, V. B. Adya, C. Affeldt, and *et al.*, *Classical and Quantum Gravity* **34**, 044001 (2017).
- [41] T. Dietrich, A. Samajdar, S. Khan, N. K. Johnson-McDaniel, R. Dudi, and W. Tichy, *Phys. Rev. D* **100**, 044003 (2019), arXiv:1905.06011 [gr-qc].
- [42] G. Ashton, M. Hübner, P. D. Lasky, C. Talbot, K. Ackley, S. Biscoveanu, Q. Chu, A. Divakarla, P. J. Easter, B. Goncharov, and *et al.*, *The Astrophysical Journal Supplement Series* **241**, 27 (2019).
- [43] P. Landry, R. Essick, and K. Chatziioannou, *Phys. Rev. D* **101**, 123007 (2020), arXiv:2003.04880 [astro-ph.HE].
- [44] C. Cutler and E. E. Flanagan, *Phys. Rev. D* **49**, 2658 (1994), arXiv:gr-qc/9402014.
- [45] J. Aasi *et al.* (LIGO Scientific, VIRGO), *Phys. Rev. D* **88**, 062001 (2013), arXiv:1304.1775 [gr-qc].
- [46] J. Calderón Bustillo, S. H. W. Leong, T. Dietrich, and P. D. Lasky, *Astrophys. J. Lett.* **912**, L10 (2021), arXiv:2006.11525 [gr-qc].
- [47] D. Adhikari *et al.* (PREX), *Phys. Rev. Lett.* **126**, 172502 (2021), arXiv:2102.10767 [nucl-ex].
- [48] B. T. Reed, F. J. Fattoyev, C. J. Horowitz, and J. Piekarewicz, *Phys. Rev. Lett.* **126**, 172503 (2021), arXiv:2101.03193 [nucl-th].
- [49] J. Xu, W.-J. Xie, and B.-A. Li, *Phys. Rev. C* **102**, 044316 (2020), arXiv:2007.07669 [nucl-th].
- [50] X. Viñas, M. Centelles, X. Roca-Maza, and M. Warda, *Eur. Phys. J. A* **50**, 27 (2014), arXiv:1308.1008 [nucl-th].
- [51] J. Alsing, H. O. Silva, and E. Berti, *Mon. Not. Roy. Astron. Soc.* **478**, 1377 (2018), arXiv:1709.07889 [astro-ph.HE].
- [52] P. Landry and J. S. Read, *Astrophys. J. Lett.* **921**, L25 (2021), arXiv:2107.04559 [astro-ph.HE].
- [53] B. S. Sathyaprakash and B. F. Schutz, *Living Rev. Rel.* **12**, 2 (2009), arXiv:0903.0338 [gr-qc].
- [54] B. P. Abbott *et al.* (LIGO Scientific, Virgo), *Class. Quant. Grav.* **37**, 055002 (2020), arXiv:1908.11170 [gr-qc].